scientific reports

Check for updates

OPEN

Ubiquitin-specific protease 14 inhibition promotes mitophagy and attenuates neural apoptosis after spinal cord injury

Dingwei Wu[1,5], Dehui Chen[1,2,5], Huina Chen[3,5], Zhengxi Yu[1,2], Hao Feng[1,4], Linquan Zhou[1], Zhi Chen[1], Tengbin Shi[1], Rongcan Wu[1], Yelei Zhang[1], Lei Sun[3], Zhenyu Wang[1]✉ & Wenge Liu[1]✉

Spinal cord injury (SCI) is a devastating condition characterized by severe neurological deficits and limited recovery, primarily due to the intricate cascade of secondary injury mechanisms. Post-SCI mitochondrial dysfunction can lead to increased oxidative stress and neuronal apoptosis. This study aimed to investigate whether inhibition of USP14 could enhance mitophagy, thereby counteracting apoptosis and providing effective neuroprotection both in vitro and in vivo after SCI. Pharmacological and genetic approaches were employed to inhibit USP14 in rat models of SCI and in HT-22 neuronal cells subjected to oxygen-glucose deprivation (OGD). The results revealed that USP14 inhibition significantly reduced neuronal apoptosis by modulating mitochondrial apoptotic pathways and preserving mitochondrial content, subsequently alleviating neurological deficits associated with SCI. Enhanced autophagic flux induced by USP14 inhibition facilitated selective clearance of damaged mitochondria, offering substantial protection to neurons and promoting functional motor recovery. Blocking mitophagy with 3-MA reversed these protective effects, underscoring the critical role of mitophagy in the neuroprotective outcomes mediated by USP14 inhibition. Collectively, our findings suggest that inhibiting USP14 enhances mitophagy, maintains mitochondrial function, and reduces neuronal apoptosis, thereby protecting neurons and improving motor function post-SCI. These results highlight USP14 as a promising therapeutic target for early intervention strategies in SCI through the modulation of mitochondrial function and enhancement of mitophagy.

Keywords USP14, USP14 inhibition, Mitophagy, Spinal cord injury, DUBs

Abbreviations

USP14	Ubiquitin-specific protease 14
SCI	Spinal cord injury
BBB	Basso, Beattie, and Bresnahan
Bcl-2	B-cell lymphoma 2
CCK-8	Cell counting Kit-8
CNS	Central nervous system
CytC	Cytochrome C
DMSO	Dimethyl sulfoxide
DUB	Deubiquitinating enzyme
H&E	Hematoxylin and eosin
LC3/LC3B	Microtubule associated protein 1 light chain 3/B
MFN2	Mitofusin-2
mtROS	Mitochondrial reactive oxygen species
OGD	Oxygen-glucose deprivation

[1]Department of Orthopedics, Fujian Medical University Union Hospital, No.29, Xin Quan Road, Fuzhou 350001, Fujian, China. [2]Department of Minimally Invasive Spinal Surgery, The Affiliated Hospital of Putian University, Putian 351100, Fujian, China. [3]School of Health, Fujian Medical University, Fuzhou 350108, Fujian, China. [4]Department of Orthopedic, Laibin People's Hospital, Laibin 546100, Guangxi, China. [5]These authors contributed equally: Dingwei Wu, Dehui Chen and Huina Chen. ✉email: zhenyu_wang@fjmu.edu.cn; wengeunion@fjmu.edu.cn

PI3K	Phosphoinositide 3-kinase
PINK1	PTEN-induced putative kinase 1
TEM	Transmission electron microscope
TUNEL	Terminal deoxynucleotidyl transferase dUTP nick end labeling
UPS	Ubiquitin-proteasome system

Spinal cord injury (SCI) is an acute form of central nervous system (CNS) trauma that continues to pose major global health challenges due to its multifaceted pathological processes, including excitotoxicity, oxidative stress, inflammation, apoptosis, and autophagy[1]. Since primary injury following SCI is largely irreversible, most current research focuses on regulating the secondary injury that ensues. Among the secondary injury, neuronal apoptosis is a critical pathological event contributing to neurological deficits[2]. Although multiple intervention strategies (e.g., controlling inflammation, reducing cell death, modulating scar formation, and regulating neurotrophic factors and angiogenesis) have shown safety and efficacy in animal models, SCI remains a formidable challenge[3].

Mitochondria play a central role in cellular metabolism by producing ATP through the mitochondrial electron transport chain and oxidative phosphorylation. Beyond energy production, they are integral to regulation of reactive oxygen species (ROS), and the induction of apoptosis[4,5]. Mitochondrial dysfunction not only increases oxidative stress but also impairs ATP generation, ultimately leading to cell death. In the context of acute SCI, mitochondria become especially vulnerable, releasing harmful quantities of ROS that trigger neural apoptosis[6]. Notably, increased mitophagy—the selective autophagic clearance of damaged mitochondria—has been demonstrated to rescue neuronal apoptosis and enhance motor function in the context of SCI[7,8].

Ubiquitin-specific protease 14 (USP14), a deubiquitinating enzyme (DUB) associated with the proteasome, exerts a dual function in controlling protein degradation. Growing evidence suggests that USP14 is involved in various canonical signaling pathways linked to neurodegenerative disorders and autophagy[9]. In particular, USP14 negatively regulates autophagy by inhibiting K63-linked ubiquitination of Beclin 1[10]. Both genetic and pharmacological inhibition of USP14 have been shown to enhance mitophagy, independent of traditional mitophagy mediators such as PINK1 and Parkin. A key mechanism underlying USP14-driven mitophagy is the exposure of Prohibitin 2, an LC3 receptor, triggered by mitochondrial fragmentation and membrane rupture. Moreover, in vivo studies demonstrate that suppressing USP14 can restore mitochondrial function and alleviate mitochondrial dysfunction[11]. These findings underscore USP14 as a promising therapeutic target for mitigating mitochondrial dysfunction and enhancing neuronal survival following SCI through the modulation of mitophagy.

This study was designed to evaluate the therapeutic potential of USP14 inhibition in both in vivo and in vitro SCI models and to investigate the underlying mechanisms, focusing on whether USP14 inhibition promotes mitophagy, thereby contributing to reduced ROS production, maintained mitochondrial membrane potential, preservation of mitochondrial function and content, and a decrease in neuronal apoptosis.

Results

USP14 inhibition promotes the recovery of rats after SCI

To assess the impact of USP14 inhibition on functional recovery after SCI, we evaluated locomotor function using the Basso, Beattie and Bresnahan (BBB) locomotor rating scale and footprint analysis. USP14 inhibitor IU1 was injected in SCI rats to inhibit the function of USP14 (Fig. 1A)[12]. At 24 h post-injury, no statistically significant difference in BBB scores was found between the SCI and SCI + IU1 treatment groups. However, starting at 3 days post-injury, rats in the SCI + IU1 group exhibited significantly improved BBB scores compared to the SCI group (Fig. 1B), indicating enhanced locomotor recovery. Footprint analysis, used to assess gait and motor coordination, revealed a marked impairment in hindlimb function in all SCI animals compared to sham controls. Consistent with the BBB scores, animals treated with IU1 (SCI + IU1 group) demonstrated significant improvement in gait and motor coordination compared to untreated SCI animals on day 7 after contusion (Fig. 1C). Histological analysis using H&E staining one week following SCI revealed substantial tissue disorganization and widespread damage within the spinal cord of SCI animals compared to sham controls. Importantly, the extent of tissue damage was notably reduced in the SCI + IU1 group compared to the SCI group (Fig. 1D). To further investigate the neuroprotective effects of USP14 inhibition, we quantified the number of surviving spinal cord anterior horn neurons using Nissl staining. Our analysis revealed a significant decrease in the number of surviving anterior horn neurons in the SCI group compared to the sham group and an increase in the number of surviving neurons in SCI + IU1 group (Fig. 1E,F). These findings suggest that USP14 inhibition provides neuroprotection and promotes functional recovery after SCI. Further studies are need to fully elucidate the mechanisms underlying the protective effects of USP14 inhibition.

USP14 inhibition inhibited apoptosis and enhanced autophagy after SCI

Neuronal apoptosis is a critical pathological event contributing to neurological deficits following SCI[2]. To investigate the effect of USP14 inhibition on apoptosis, TUNEL staining was performed and showed more apoptotic cells in the SCI group, while USP14 inhibition decreased the apoptosis rate (Fig. 2A,C). In addition, Western blot analysis was conducted to measure the protein levels of pro-apoptotic factors (Bax, cleaved caspase-3, and cleaved caspase-9) as well as anti-apoptotic factors (Bcl-2, caspase-3, and caspase-9). The extent of apoptosis was assessed by calculating the ratios between pro- and anti-apoptotic protein expression levels. Compared to the sham group, the SCI group exhibited increased ratios of Bax/Bcl-2, cleaved caspase-3/caspase-3, and cleaved caspase-9/caspase-9. Notably, USP14 inhibition significantly reversed these changes (Fig. 2B,D–F), suggesting that USP14 inhibition exerts neuroprotective effects by suppressing apoptosis after SCI.

We next found an increased autophagy rate by measuring the protein levels of the autophagy marker LC3B (LC3B-II/LC3B-I ratio) and the autophagic flux marker p62 using Western blotting. SCI induced an increase

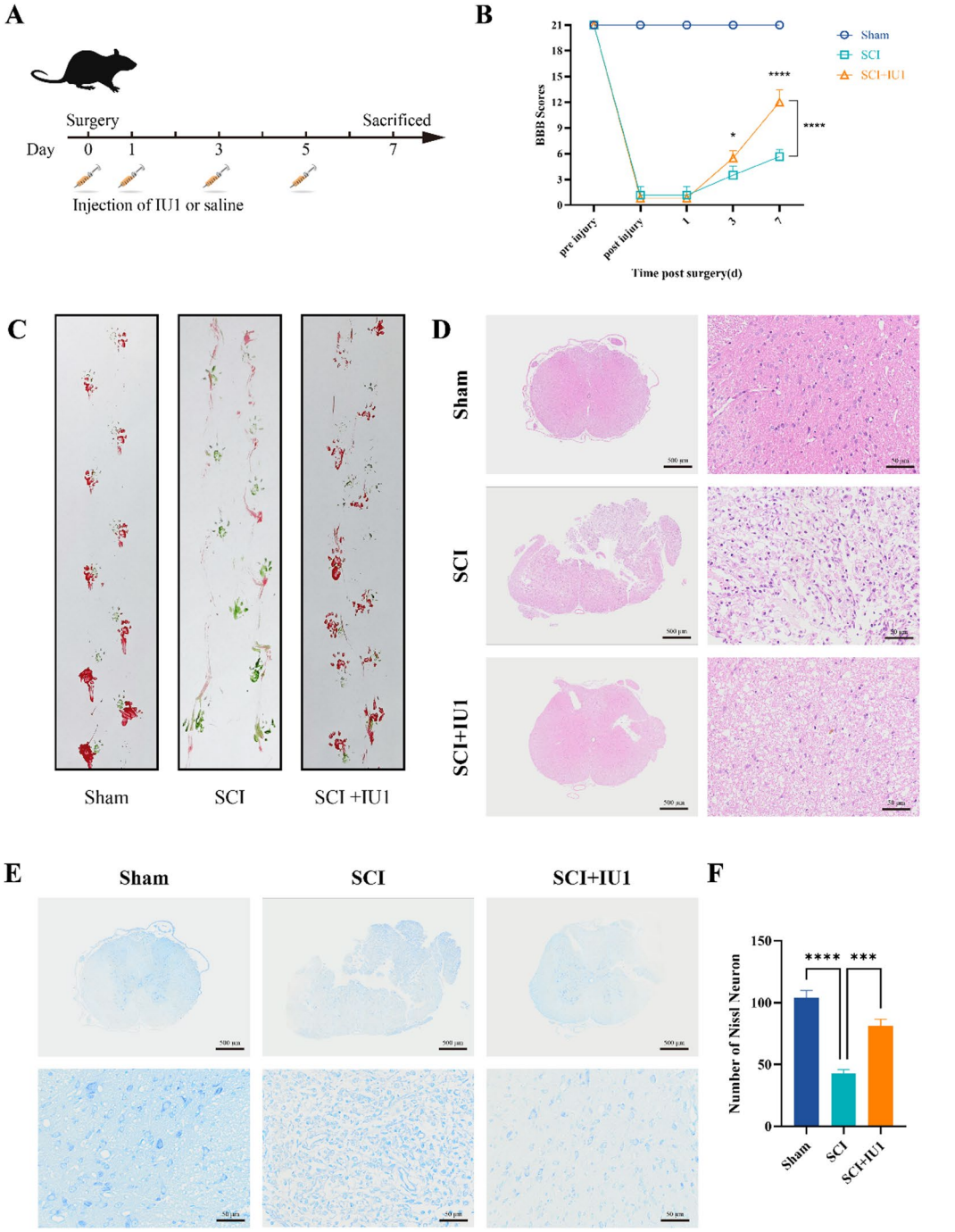

Fig. 1. USP14 inhibition facilitates recovery of rats after SCI. (**A**) Timeline of animal experiments, indicating the timing of IU1 injections (100 μM, 2 mL for each) and tissue collection. (**B**) BBB scores measured at various time points following spinal cord contusion across different rat groups (mean ± SD, $n = 6$). (**C**) Example of rat footprints recorded one week after SCI. Green indicates forelimb prints, and red indicates hindlimb prints. (**D**) Representative images of cross-sectional H&E staining of the spinal cord from each experimental group ($n = 3$). Scale bar = 500 μm–50 μm. (**E**,**F**) Nissl staining was used to quantify the number of surviving neurons in each field of view across the groups (mean ± SD, $n = 3$). Scale bar = 500 μm–50 μm. Statistical analysis was performed using two-way ANOVA for BBB score and one-way ANOVA for Nissl staining to determine p-values for mean ± standard deviation from three independent experiments. * $p < 0.05$, *** $p < 0.001$, **** $p < 0.0001$.

in the LC3B-II/LC3B-I ratio and a decrease in p62 levels. USP14 inhibition further enhanced these changes, indicating that USP14 inhibition promotes autophagy following SCI (Fig. 2B,G,H). Immunofluorescence analysis of LC3B and NeuN further confirmed these results (Fig. 2I,J), suggesting that the higher autophagy rate in SCI + IU1 group may further improve the recovery of neurons after SCI.

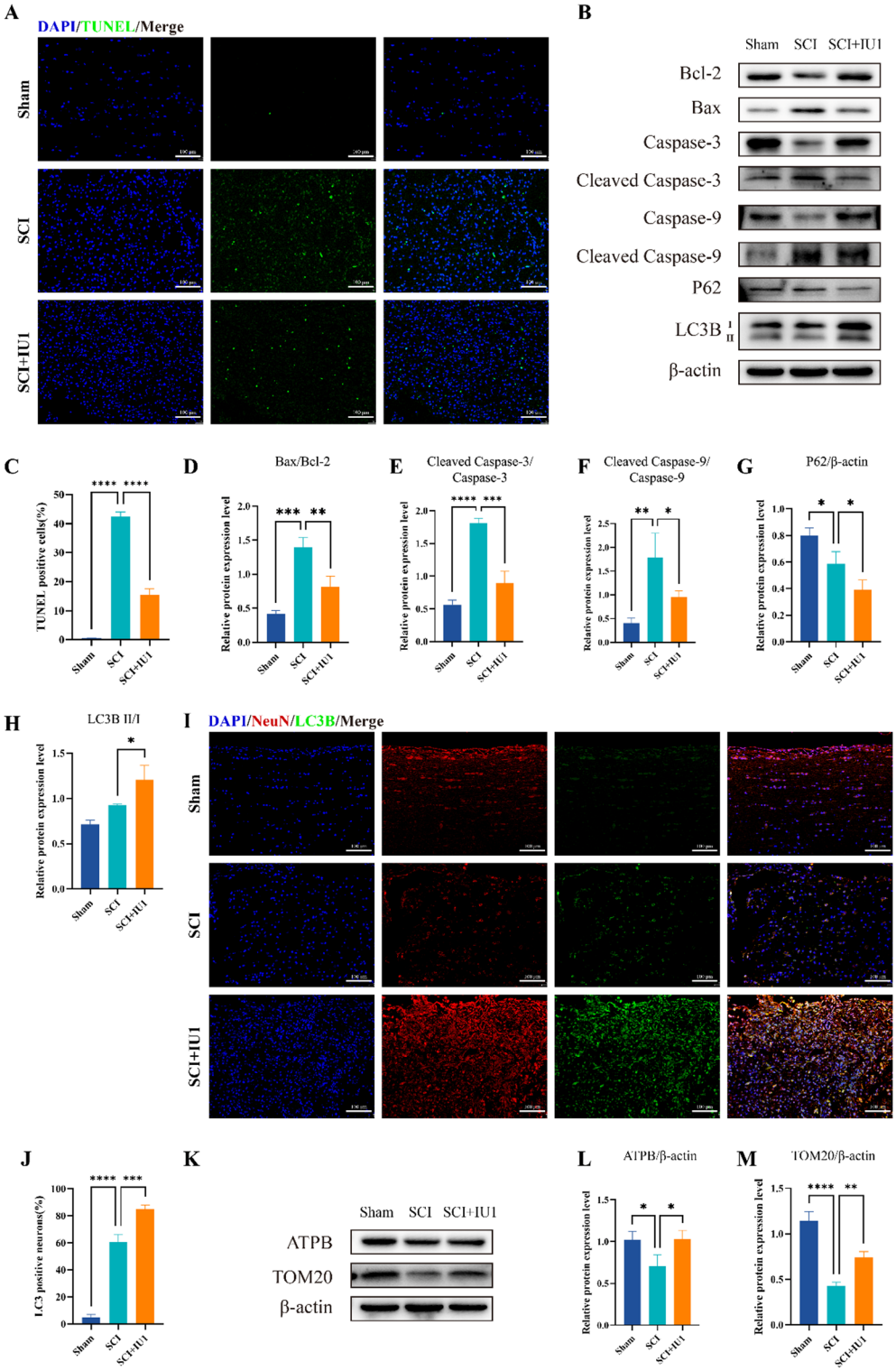

Fig. 2. USP14 inhibition reduces apoptosis and enhances autophagy post-SCI. (**A**,**C**) TUNEL staining of spinal cord sections, with statistical analysis of the percentage of TUNEL-positive cells (mean ± SD, $n = 3$). Scale bar = 100 μm. (**B**,**D**–**F**) Western blotting and semi-quantitative analysis of apoptosis-related proteins (Bax/Bcl-2, Cleaved-caspase-3/Caspase-3, Cleaved-caspase-9/Caspase-9) following SCI. (**B**,**G**–**H**) Western blotting and semi-quantitative analysis of autophagy-related proteins (p62, LC3B- Ⅰ / Ⅱ) following SCI. (I) Representative images of transverse spinal cord sections stained with anti-LC3B (green) and anti-NeuN (red) antibodies, with DAPI (blue) for nuclear staining. Scale bar = 100 μm. (**J**) Quantification of LC3-positive neurons in the injury area. (K-M) Western blotting and semi-quantitative analysis of mitochondrial proteins ATPB and TOM20 following SCI. Data were analyzed using one-way ANOVA to calculate p-values for the mean ± standard deviation from three independent experiments. * $p < 0.05$, ** $p < 0.01$, *** $p < 0.001$, **** $p < 0.0001$.

To evaluate mitochondrial content, we also measured total mitochondrial content by the protein levels of the mitochondrial inner membrane protein ATPB and the outer membrane protein TOM20. SCI resulted in a decrease in total mitochondrial volume, which was restored in the SCI + IU1 group (Fig. 2K–M). Our findings suggest that the increased autophagy levels may facilitate the recovery of mitochondrial function and content. However, the involvement of mitophagy still requires further investigation.

USP14 inhibition reduces apoptosis in the in vitro OGD model

To investigate the protective effects of USP14 inhibition and its underlying mechanisms in SCI, we utilized an in vitro oxygen-glucose deprivation (OGD) model, which can effectively mimic the extracellular environment during the early stages of SCI[13,14]. HT-22 cells were selected for these in vitro experiments due to their common use in SCI research[15,16]. A concentration of 50 μM IU1 was chosen for cell experiments based on CCK-8 assays (Supplementary Fig. 1A). We then examined the effect of different OGD durations on cell viability. The survival rate of OGD + IU1-treated cells was significantly higher than that of the OGD group at 6 h (Supplementary Fig. 1B). Therefore, a 6 h OGD period was used for subsequent in vitro experiments.

Western blot analysis revealed that OGD significantly upregulated the expression of USP14. Additionally, OGD treatment resulted in increased ratios of Bax/Bcl-2, cleaved caspase-3/caspase-3, and cleaved caspase-9/caspase-9, indicating an elevated apoptosis rate. Inhibition of USP14 with IU1 significantly reversed these changes, suggesting that USP14 plays a crucial role in mediating OGD-induced apoptosis (Fig. 3A,B).

To further investigate the role of USP14, we generated a stable HT-22 cell line with USP14 gene knockdown (sh-USP14) using lentiviral transduction. Knockdown efficiency was confirmed by Western blotting. USP14 expression was significantly lower in the sh-USP14 group compared to both the control group and the vector control group (Supplementary Fig. 2A, B). Consistent with our previous findings, Western blot analysis demonstrated that USP14 knockdown significantly attenuated the apoptotic level of HT-22 cells induced by OGD (Fig. 3C,D). Furthermore, flow cytometric analysis demonstrated a significantly higher proportion of apoptotic cells in the OGD group compared to the control group. Although the proportion of apoptotic cells in the OGD + sh-USP14 group was also increased relative to the control, it was substantially lower than that observed in the OGD group (Fig. 3E,F). Taken together, these results suggest that both pharmacological inhibition and genetic knockdown of USP14 reduce apoptosis following OGD treatment.

USP14 inhibition alleviated OGD-induced mitochondrial dysfunction in vitro

Spinal cord neurons are particularly vulnerable to SCI due to their high metabolic and energetic demands. Mitochondria, primary targets of ischemic injury, play a pivotal role in the pathogenesis of SCI[17]. Therefore, we explored whether USP14 inhibition could confer protective effects on mitochondrial function beyond its established inhibitory role in the mitochondrial apoptotic pathway. Mitochondrial membrane potential (ΔΨm) was assessed using JC-1 staining. OGD significantly reduced ΔΨm, an effect that was significantly reversed by USP14 knockdown (Fig. 4A,B). Additionally, measurement of mitochondrial reactive oxygen species (mtROS) production indicated a substantial elevation in mtROS levels following OGD treatment; however, USP14 knockdown significantly attenuated this effect (Fig. 4C,D). Collectively, these findings suggest that USP14 inhibition preserves mitochondrial function by stabilizing mitochondrial membrane potential and reducing mtROS accumulation, thereby alleviating oxidative stress-induced mitochondrial dysfunction and subsequent apoptosis in vitro.

USP14 inhibition modulated mitochondrial function and apoptosis through enhancing mitophagy

Mitophagy, a selective form of autophagy targeting damaged mitochondria, is crucial for maintaining mitochondrial function and mitigating apoptosis under stress conditions[18–20]. We investigated whether the neuroprotective effect of USP14 inhibition is mediated by mitophagy.

To confirm the role of USP14 in mitophagy, we conducted a series of in vitro experiments. Western blot analysis demonstrated that OGD significantly increased the LC3B-II/LC3B-I ratio and decreased p62 expression, indicative of enhanced autophagy. These changes were further augmented by USP14 knockdown. Additionally, the elevated autophagy levels observed in both the sh-USP14 group and the OGD + sh-USP14 group, coupled with a reduction in ATPB and TOM20 protein levels in the sh-USP14 group, suggest the induction of mitophagy. Furthermore, inhibition of USP14 successfully attenuates the OGD-induced loss of mitochondrial content following OGD-induced injury (Fig. 5A-E).

Transmission electron microscopy (TEM) was employed to directly visualize autophagic structures, including autophagosomes (with or without mitochondria) and autophagolysosomes[21,22]. Compared to the control group, the OGD group exhibited a significant increase in damaged and swollen mitochondria (red arrows) and autophagosomes (blue arrows). Furthermore, both the sh-USP14 group and the OGD + sh-USP14 group exhibited higher numbers of mitophagosomes (yellow arrows) compared to the control and OGD groups, with the highest number observed in the OGD + sh-USP14 group (Fig. 5F, G). These findings demonstrate that USP14 inhibition effectively promotes mitophagy. Additionally, the OGD + sh-USP14 group showed an increased abundance of healthy mitochondria relative to the OGD group, highlighting the protective role of USP14 inhibition in preserving mitochondrial integrity (Fig. 5F).

To further assess mitophagy, we conducted immunofluorescence experiments analyzing the colocalization of ATPB (a mitochondrial marker) and LC3 (an autophagosome structural protein). OGD treatment significantly elevated LC3 puncta formation and its colocalization with mitochondria, indicating increased LC3 expression and mitochondrial association. Knockdown of USP14 further intensified these effects. Quantitative analysis of colocalization, represented as the number of yellow puncta and their proportion relative to the total mitochondrial content (%) per cell, confirmed a significant increase in the OGD + sh-USP14 group compared

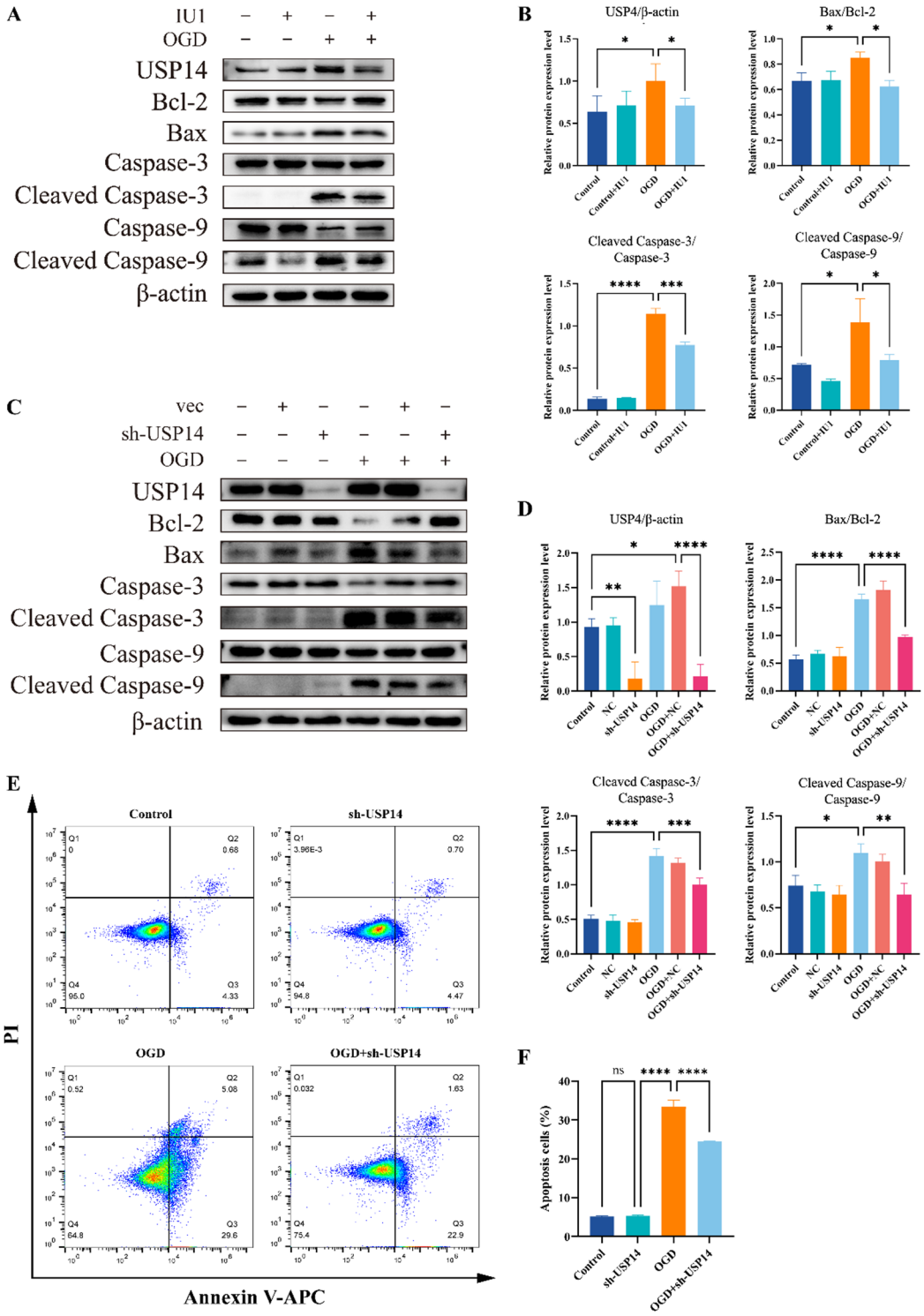

Fig. 3. USP14 inhibition protects neuronal activity from OGD-induced damage in vitro. (**A**,**B**) HT-22 cells were treated with IU1 (50 μM), followed by Western blotting and semi-quantitative analysis of USP14 and apoptosis-related proteins (Bax/Bcl-2, Cleaved-caspase-3/Caspase-3, Cleaved-caspase-9/Caspase-9) post-OGD. (**C**,**D**) Stable HT-22sh-USP14 cell lines were generated, and Western blotting and semi-quantitative analysis were performed to evaluate the expression of USP14 and apoptosis-related proteins following OGD. (**E**) Annexin V-APC/PI double staining combined with flow cytometry was used to assess apoptosis in HT-22 cells with or without USP14 knockdown. (**F**) Quantification of apoptotic HT-22 cells with USP14 knockdown or control. Statistical analysis was performed using two-way ANOVA to determine p-values for the mean ± standard deviation from three independent experiments. ns $p > 0.05$, * $p < 0.05$, ** $p < 0.01$, *** $p < 0.001$, **** $p < 0.0001$.

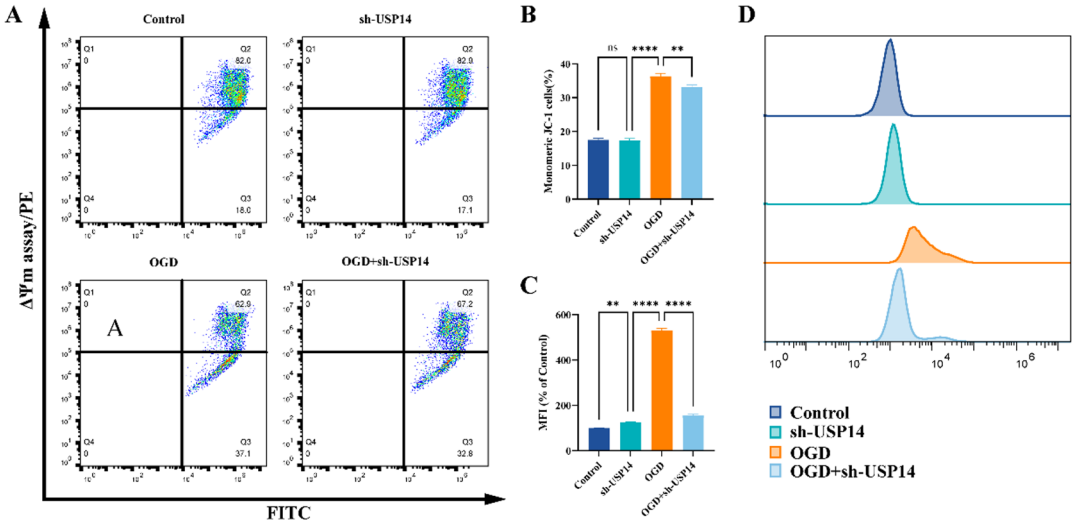

Fig. 4. USP14 inhibition ameliorates oxidative stress-induced mitochondrial dysfunction in vitro. (**A**,**B**) Flow cytometry was used to measure mitochondrial membrane potential by JC-1 staining to assess mitochondrial function (mean ± SD, $n = 3$). (**C**,**D**) Flow cytometry was used to measure mitochondrial ROS (mtROS) levels in cells from each group (mean ± SD, $n = 3$). Statistical analysis was performed using two-way ANOVA to calculate p-values for the mean ± standard deviation from three independent experiments. ns $p > 0.05$, ** $p < 0.01$, **** $p < 0.0001$.

to the OGD group (Fig. 5H–J). These results provide compelling evidence that USP14 inhibition promotes mitophagy. Furthermore, OGD induced marked mitochondrial fragmentation (Fig. 5H), evidenced by a shorter mean branch length per mitochondrion (Supplementary Fig. 3A) and a lower form factor (Supplementary Fig. 3B), suggesting increased mitochondrial fission and dysfunction following OGD[23–25]. Notably, mitochondrial morphology in the OGD + sh-USP14 group exhibited substantial improvement, closely resembling that observed in the control group. Collectively, these observations illustrate that USP14 inhibition protects neuronal mitochondria by enhancing mitophagy, thereby mitigating spinal cord neuronal damage induced by OGD.

To further explore the interplay between USP14, mitochondria, autophagy, and apoptosis, we used 3-methyladenine (3-MA; Sigma, U.S.A), a widely used inhibitor of autophagy that blocks autophagosome formation by inhibiting type III phosphatidylinositol 3-kinase (PI3K)[26]. In the presence of 3-MA, USP14 knockdown no longer decreased the ratios of Bax/Bcl-2, cleaved caspase-3/caspase-3, and cleaved caspase-9/caspase-9 following OGD. Instead, 3-MA significantly attenuated the effects of USP14 knockdown on these apoptotic markers. Furthermore, treatment with 3-MA significantly decreased the expression levels of mitochondrial proteins ATPB and TOM20 in the OGD + sh-USP14 group, indicating that 3-MA attenuated the mitochondrial protective effects conferred by USP14 knockdown (Fig. 6A, B). These results demonstrate that inhibition of USP14 rescues OGD-induced apoptosis through the enhancement of mitophagy.

Discussion

SCI is a debilitating neurological condition characterized by significant functional deficits and elevated mortality rates. The majority of SCI cases are traumatic SCI, frequently resulting from motor vehicle accidents, acts of violence, sports-related incidents, or falls[27,28]. While global age-standardized incidence, prevalence, and years lived with disability (YLDs) due to SCI have generally declined, a gradual increase from a lower baseline has been observed in regions with lower Socio-Demographic Index (SDI)[29]. Consequently, research focused on SCI repair remains of paramount importance. SCI pathogenesis involves both primary and secondary injury. Primary injury directly damages the spinal cord and causes vascular disruption, triggering extensive apoptosis and necrosis, ultimately culminating in spinal cord ischemia and initiating a cascade of secondary injury events[30]. Although primary damage is often unavoidable, the secondary injury phase presents a potential therapeutic window due to its relative reversibility[31]. Therefore, early intervention is crucial for mitigating SCI progression, preventing secondary damage, and promoting tissue repair. This study investigated the role of USP14 inhibition in the acute phase of SCI and explored its underlying mechanisms. Our findings demonstrate that early USP14 inhibition confers protection against SCI and facilitates the repair process. Specifically, USP14 inhibition enhanced mitophagy to improve mitochondrial function and reduce mitochondria-dependent apoptosis in both an in vivo rat SCI model and an in vitro OGD model.

Mitochondria generate approximately 90% of cellular ATP through oxidative phosphorylation, a process essential for maintaining neuronal homeostasis, function, and survival[32,33]. However, mitochondrial metabolism is intrinsically linked to the production of ROS, rendering mitochondria susceptible to damage. Excessive ROS accumulation can trigger the mitochondrial apoptotic pathway, leading to neuronal apoptosis following acute central nervous system (CNS) injuries such as SCI[1,6,34]. This accumulation of ROS can further compromise ΔΨm and increase mitochondrial membrane permeability. These alterations promote the release of cytochrome

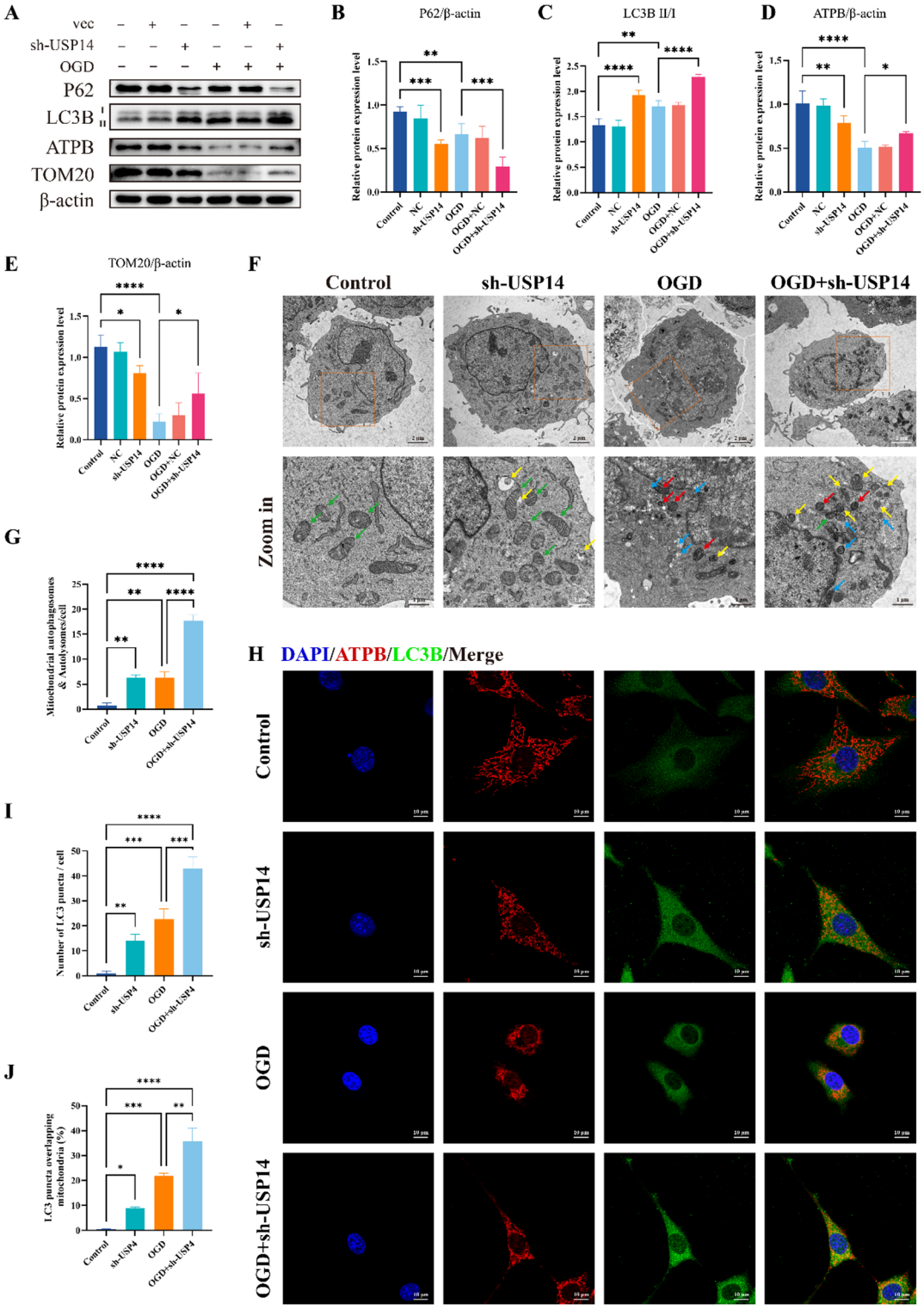

Fig. 5. USP14 inhibition enhances mitophagy, modulating mitochondrial function and apoptosis. (**A**–**E**) Western blot and semi-quantitative analysis of LC3B II/I, P62, ATPB, and TOM20 expression (mean ± SD, $n = 3$). (**F**–**G**) TEM analysis of cellular autophagy. The boxed regions in the upper panels are magnified in the lower panels. Green arrows indicate healthy mitochondria, red arrows indicate damaged mitochondria, blue arrows point to autophagosomes, and yellow arrows show mitophagosomes. (**H**–**J**) Co-localization of ATPB with LC3 was observed via laser confocal microscopy to assess mitochondrial autophagy. ATPB is marked with red fluorescence, LC3 with green fluorescence, and the yellow fluorescence represents co-localization. All cell nuclei are stained with DAPI (blue). Quantification of yellow puncta in each group (mean ± SD, $n = 3$). Scale bar = 20 μm. Statistical analysis was performed using two-way ANOVA to calculate p-values for the mean ± standard deviation from three independent experiments. ns $p > 0.05$, * $p < 0.05$, ** $p < 0.01$, *** $p < 0.001$, **** $p < 0.0001$.

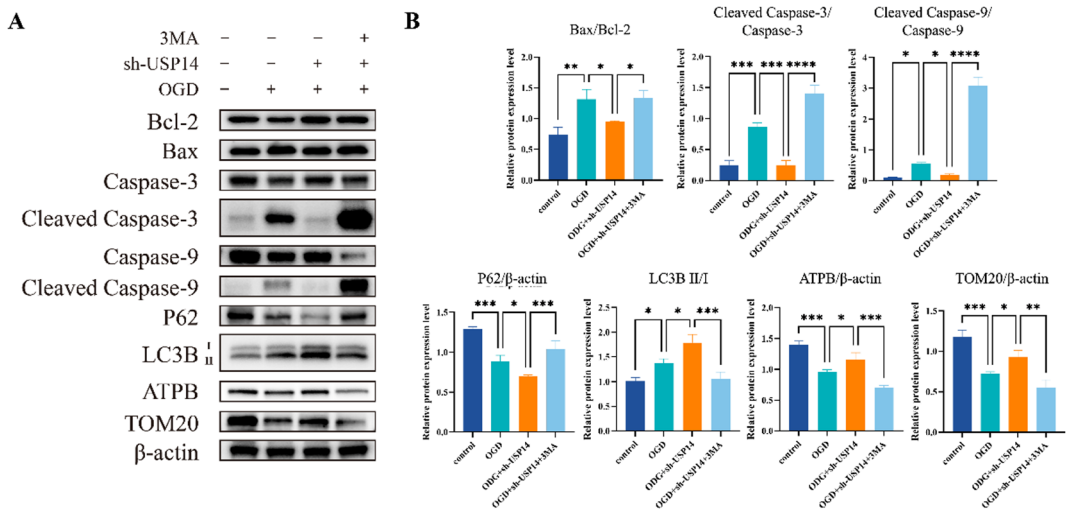

Fig. 6. 3-MA inhibits the protective effects of USP14 inhibition against mitochondrial dysfunction and apoptosis. (**A**,**B**) Western blotting and semi-quantitative analysis of apoptosis-related proteins (Bax/Bcl-2, Cleaved-caspase-3/Caspase-3, Cleaved-caspase-9/Caspase-9), autophagy-related proteins (LC3B II/I, P62), and mitochondrial-related proteins (ATPB, TOM20) following OGD and 3-MA treatment (mean ± SD, $n = 3$). Statistical analysis was performed using one-way ANOVA to determine p-values for the mean ± standard deviation from three independent experiments. * $p < 0.05$, ** $p < 0.01$, *** $p < 0.001$, **** $p < 0.0001$.

c (CytC) and other pro-apoptotic factors, accelerate the formation of apoptotic vesicles, and initiate the caspase cascade, ultimately culminating in apoptosis[35]. Our findings corroborate these observations, demonstrating elevated mtROS levels and a concomitant decrease in ΔΨm in cells subjected to OGD. Concurrently, we observed a significant upregulation in the ratios of apoptosis-associated proteins, specifically Bax/Bcl-2, cleaved caspase-3/caspase-3, and cleaved caspase-9/caspase-9. Neuronal survival and function are critically dependent on mitochondrial structural integrity, number, and activity[36]. Notably, mitochondrial function undergoes significant changes immediately within 2–8 h after SCI and persists for at least 24 h[37], with increased mitochondrial fission contributing to excessive fragmentation and neuronal apoptosis. This underscores the importance of early intervention in SCI. Maintaining mitochondrial homeostasis is therefore paramount for neuronal survival in this context. Effective and timely interventions targeting mitochondrial injury are a key strategy to prevent neuronal death and maximize neurological function preservation after SCI. In our study, we observed that USP14 inhibition attenuated mtROS production and preserved ΔΨm, thereby mitigating a key driver of early mitochondrial damage. USP14 inhibition also decreased the ratio of Bax/Bcl-2, cleaved caspase-3/caspase-3 and cleaved caspase-9/caspase-9, indicating suppression of the mitochondrial apoptosis pathway.

Mitophagy, a selective form of autophagy, specifically targets and degrades damaged mitochondria[38]. As a critical mitochondrial quality control (MQC) mechanism, mitophagy plays a crucial role in regulating mitochondrial function and mitochondrial apoptotic pathway following SCI[19,39,40]. Several studies have demonstrated that early mitophagy can restore mitochondrial function and mitigate mitochondrial apoptosis, thereby protecting cells from ischemic injury. For instance, sustained tacrolimus release promotes mitophagy via the FKBP52/AKT pathway, alleviating the apoptosis and enhancing MQC, axonal growth, neural regeneration, and motor recovery after SCI[41]. Similarly, zinc ions mitigate oxidative stress-induced MQC dysfunction by inhibiting the Lgals3-Bax pathway, thereby promoting neuronal mitophagy and mitigating neuronal apoptosis[19]. Ligustilide (LIG) has also been found to reverse oxidative stress-induced downregulation of BNIP3 and enhance mitophagy through BNIP3-LC3 interaction, ultimately alleviating mitochondrial dysfunction and reducing neuronal apoptosis both in vitro and in vivo[21]. In our study, we observed that USP14 inhibition increased the LC3B II/I ratio, promoted LC3B recruitment to mitochondria, and decreased p62 expression, along with the expression of mitochondrial proteins ATPB and TOM20. These findings confirm that USP14 inhibition regulates mitophagy after SCI. Furthermore, USP14 inhibition preserved mitochondrial content following both in vitro OGD injury and in vivo SCI. This preservation likely reflects enhanced mitophagy that accelerates the clearance of damaged mitochondria, thereby maintaining mitochondrial homeostasis, supporting function, and limiting net loss of mitochondrial content.

Deubiquitinating enzymes (DUBs) play a crucial role in regulating the ubiquitin system by reversing ubiquitin modifications[42,43]. Many DUBs function as important regulators of autophagy, including USP33, USP30, USP22, USP15, and USP14. Current research on the relationship between DUBs and autophagy has primarily focused on studies related to Parkinson's disease (PD) and ischemia-reperfusion injury. These studies indicate that DUBs can influence autophagy by regulating Parkin stability, either through direct interaction or by antagonizing Parkin activity (indirect interaction)[44,45]. For example, USP33 preferentially removes K6, K11, K48, and K63-linked ubiquitin conjugates from Parkin, especially at Lys435, and its inhibition enhances Parkin stability, mitochondrial recruitment, mitophagy, and neuronal protection[46]. Similarly, ruthenium red (RR) has been shown to attenuate post-resuscitation myocardial dysfunction (PRMD) by promoting mitophagy

through USP33 inhibition[47]. Similarly, USP30 inhibition promotes mitophagy, protecting against PD-associated behavioral deficits and reducing ROS accumulation[48,49]. In the context of subarachnoid hemorrhage (SAH), USP30 inhibition promotes mitophagy by enhancing Parkin-mediated ubiquitination of mitochondrial fusion protein 2 (MFN2), promoting mitochondrial clearance and reducing apoptosis[50].

In studies of PD, USP14 inhibition has been shown to enhance mitophagy, leading to increased lifespan and rescue of the pathological phenotype in two Drosophila models of PD[11]. Further investigation in mammalian neurons revealed that USP14 inhibition specifically promotes mitochondrial autophagy in induced neurons (iNeurons). Notably, the mitophagy effect of USP14 inhibition depends on the expression of the mitochondrial E3 ubiquitin ligase MITOL/MARCH5, rather than PINK1/Parkin[51]. In the context of neonatal hypoxic-ischemic encephalopathy (HIE), disease progression is associated with activated Hippo signaling, which enhances Yap1 phosphorylation at Ser-127 but inhibits Yap1 protein levels. This, in turn, potentiates Usp14 transcription and leads to downregulated Lys-63 ubiquitination of Beclin-1, a key molecule in autophagy. Consequently, neuronal mitophagy is suppressed, resulting in impaired clearance of damaged neurons and potentially contributing to dysregulation of brain functions[52]. Similarly, we found that USP14 inhibition not only enhanced mitophagy but also inhibited the mitochondrial pathway of apoptosis and improved mitochondrial function, thereby protecting spinal cord neurons from SCI. Additionally, 3-MA's inhibition of autophagy attenuated the protective effects of USP14 knockdown against apoptosis and mitochondrial dysfunction. These findings confirm that the protective effects of USP14 inhibition against apoptosis and mitochondrial dysfunction are mediated through mitophagy.

This study demonstrated that early intervention of USP14 inhibition enhances mitophagy, reduces early apoptosis, and improves mitochondrial function after SCI. However, this study has several limitations. First, the specific upstream and downstream signaling molecules and pathways involved in USP14-mediated mitophagy were not fully elucidated. Second, while HT-22 cells were used for in vitro experiments, primary spinal cord neurons would have provided a more physiologically relevant model. Third, while mitophagy is widely recognized as an early defense mechanism for neuronal health after CNS injury, the threshold defining "excessive" mitophagy remains unclear, as both insufficient and excessive mitophagy can exacerbate detrimental outcomes. This study does not explore this crucial aspect of mitophagy regulation.

In conclusion, this study provides evidence that USP14 inhibition confers neuroprotection in SCI by modulating key mitochondrial processes: enhancing mitophagy, improving overall mitochondrial function and inhibiting the mitochondrial apoptotic pathway. These findings highlight USP14 as a potential therapeutic target for early intervention aimed at mitigating SCI pathology.

Materials and methods

Animals and experimental groups

All experimental procedures were approved by the Animal Ethics Committee of Fujian Medical University (approval number: IACUC FJMU 2024 – 0137) and conducted in accordance with the ARRIVE guidelines and the National Institutes of Health Guide for the Care and Use of Laboratory Animals. Adult male Sprague-Dawley rats (220–250 g, specific pathogen-free grade) were obtained from Shanghai SLAC Laboratory Animal Co. Animals were housed under standard laboratory conditions (22–24 °C, 45–55% humidity, 12-hour light/dark cycle, 4–5 rats per cage) with ad libitum access to food and water. Thirty rats were randomly assigned to three groups ($n = 10$ per group): sham, SCI, and SCI + IU1 group. In the event of death or surgical complications, affected animals were replaced. IU1 (MedChemExpress, U.S.A.) was prepared as a 100 mM stock solution in DMSO and subsequently diluted in saline to a final concentration of 100 μM. Rats in the SCI + IU1 group received intraperitoneal injections of IU1 (280 μg/kg) immediately and on days 1, 3, and 5 post-SCI[53,54]. Both sham and SCI groups received intraperitoneal injections of saline containing the same concentration of DMSO at the corresponding time points. All rats were euthanized on day 7.

Construction of SCI model in rats

SCI was induced using a modified Allen's method to ensure reproducible injury. Rats were anesthetized with an intraperitoneal injection of 1% pentobarbital sodium (50 mg/kg). After a T10 laminectomy, rats were positioned in a modified Allen's impactor (RWD Life Science Corp, 68097, U.S.A.), ensuring precise alignment of the T10 spinal cord segment beneath the impact point. A 15 g impactor with a 2.5 mm diameter flat tip was released from a height of 10 cm onto the exposed dura. The impactor was held in place for 3 min to standardize the duration of compression. Successful SCI induction was determined by the immediate presence of tail spasms and complete bilateral hindlimb paralysis. To prevent post-operative infection, rats received daily intraperitoneal injections of cefuroxime sodium (100 mg/kg) for three days. Bladders were manually expressed twice daily until spontaneous voiding returned.

Assessment of motor ability

Motor function was evaluated using the 21-point Basso, Beattie, and Bresnahan (BBB) locomotor scale[55,56]. Two blinded investigators conducted behavioral assessments at multiple time points: prior to surgery (baseline), immediately post-surgery, and on days 1, 3 and 7 following SCI. Each assessment session involved observing the rats' hindlimb movements in an open field environment for a duration of five minutes every morning during the testing period. During these observations, the investigators focused on several key parameters, including the presence of isolated joint movements, uncoordinated stepping patterns, and the coordination between forelimbs and hindlimbs. These criteria are critical for accurately determining the extent of motor impairment and recovery in the SCI model. Additionally, the BBB score was recorded immediately after each rat regained consciousness following anesthesia. Rats that exhibited BBB scores higher than 5 at any assessment point were deemed to have failed the SCI modeling process. Such rats were excluded from the study, and replacement animals were utilized to ensure consistent group sizes and the integrity of the experimental results.

On day 7 post-surgery, gait and motor coordination were assessed using a footprint analysis method. Each rat's forelimbs and hindlimbs were coated with green and red non-toxic dyes, respectively. Engineering drawings were placed flat on a tabletop, and a three-sided tunnel was constructed to guide the rats to walk forward. Rats were positioned at the tunnel entrance and encouraged to traverse it, leaving distinct footprints on the drawings. The footprint patterns were analyzed to evaluate stride length, paw placement accuracy, limb coordination, and symmetry between forelimb and hindlimb movements.

Spinal cord tissue processing and H&E and Nissl staining

One week post-SCI, rats were deeply anesthetized and transcardially perfused with 0.9% saline followed by 4% paraformaldehyde (PFA) in 0.1 M phosphate buffer. Spinal cords were harvested immediately after perfusion and post-fixed in 4% PFA overnight before paraffin embedding. Paraffin Section (4 μm) were cut and mounted on poly-L-lysine-coated slides. Hematoxylin and eosin (H&E) and Nissl staining were performed for histopathological analysis. Images were acquired using an Olympus SLIDEVIEW VS200 research slide scanner. The number of surviving neurons was quantified using ImageJ.

TUNEL assay

TUNEL staining was performed on deparaffinized sections to assess apoptosis. Sections were processed according to the manufacturer's instructions for the TUNEL assay (Elabscience, China). Nuclei were counterstained with DAPI (Genview, U.S.A.). Images were acquired using a fluorescence inverted microscope (Leica, DMi8). The number of TUNEL-positive DAPI-positive cells was quantified using ImageJ. The apoptotic index was calculated as the ratio of TUNEL-positive cells to the total number of DAPI-positive cells.

Immunofluorescence microscopy

Dewaxed spinal cord sections and fixed HT-22 cells were permeabilized with 0.2% Triton X-100 (Beyotime, China) and blocked with Blocking Buffer for Immunol Staining (Beyotime, China) for 15 min. For immunofluorescence labeling, spinal cord sections were incubated overnight at 4 °C with primary antibodies against LC3B (1:200 dilution, Abcam, ab192890) and NeuN (1:200 dilution, Abcam, ab177487). Concurrently, HT-22 cells were incubated overnight at 4 °C with primary antibodies against LC3B (1:200 dilution, Abcam, ab192890) and ATPB (1:200 dilution, Abcam, ab14730). After three washes with phosphate-buffered saline containing 0.1% Tween-20 (PBST), both sections and cells were incubated with appropriate Alexa Fluor 488- or Alexa Fluor 555-conjugated secondary antibodies (1:200 dilution, Abcam) for 1 h at room temperature. Nuclei were then counterstained with DAPI for 5 min. Images were acquired using a fluorescence inverted microscope (Leica, DMi8) and a confocal laser scanning microscope (Leica TCS SP8). Identical imaging parameters were used for all samples to ensure comparability between groups. ImageJ was used for image analysis and quantification. Mitochondria Analyzer was used to quantify the mitochondrial morphology[57].

Western blotting

Total protein was extracted from cells and tissues using RIPA lysis buffer (Beyotime Biotechnology, China) supplemented with phenylmethylsulfonyl fluoride (PMSF), phosphatase inhibitors, and protease inhibitors. Protein concentrations were determined using a BCA protein assay kit (Boost Biotechnology, China). Equal amounts of protein were separated by sodium dodecyl sulfate-polyacrylamide gel electrophoresis (SDS-PAGE) and transferred to PVDF membranes. Membranes were blocked with 5% non-fat dry milk (BioFroxx, Germany) in Tris-buffered saline with 0.1% Tween-20 (TBST) for 3 h at room temperature and then incubated overnight at 4 °C with primary antibodies against the following proteins: anti-USP14 (1:2000, Proteintech, 14517-1-AP), anti-Bax (1:1000, CST, #5023), anti-Bcl2 (1:1000, Abcam, ab692), anti-Caspase-3 (1:1000, CST, #9662), anti-Cleaved Caspase-3 (1:1000, CST, #9664), anti-Caspase-9 (1:1000, CST, #9508), anti-Cleaved Caspase-9 (1:1000, CST, #20750), anti-LC3B (1:1000, Abcam, ab192890), anti-p62 (1:1000, CST, #8025), anti-TOM20 (1:1000, Abcam, ab56783), anti-ATPB (1:2000, Abcam, ab14730), anti-β-actin(1:20000, Proteintech, 66009-1-Ig). After washing with TBST, membranes were incubated with horseradish peroxidase (HRP)-conjugated secondary antibodies (1:5000, Dingguo Biotechnology, China) for 1 h at room temperature. Protein bands were detected using an enhanced chemiluminescence (ECL) reagent (Genview, U.S.A.) and visualized with a chemiluminescence imaging system (ChemiDoc Touch, Bio-Rad, U.S.A.). The band intensity was quantified using ImageJ software, and the relative protein expression levels were normalized to the internal control (β-actin).

Cell culture and OGD model construction

Mouse hippocampal neuronal HT-22 cells (obtained from the Cell Bank of the Chinese Academy of Sciences, China) were cultured in Dulbecco's Modified Eagle's Medium (DMEM; Gibco, U.S.A.) supplemented with 10% fetal bovine serum (FBS; TOCYTO, U.S.A.) and 1% penicillin/streptomycin (Gibco, U.S.A.). Cells were maintained in a humidified CO_2 incubator (Thermo Fisher Scientific, U.S.A.) at 37 °C under a humidified atmosphere of 5% CO_2 in air and 70–80% relative humidity. To mimic the ischemic and hypoxic conditions observed after SCI, an oxygen-glucose deprivation (OGD) model was employed. Prior to OGD induction, the cell culture medium was replaced with glucose-free Hank's Balanced Salt Solution (HBSS; Genview, U.S.A.). OGD was induced by incubating cells in a hypoxic incubator (Whitley H35 Hypoxystation, Don Whitley Scientific, England) maintained at 37 °C, 70–80% relative humidity, and an atmosphere of 1% O_2, 94% N_2, and 5% CO_2. In the OGD + IU1 group, cells were pretreated with 50 μM IU1 (MedChemExpress, U.S.A.) for 24 h before the initiation of OGD. In the OGD + sh-USP14 + 3-MA group, HT-22$^{sh-USP14}$ cells were cocultured with 3-MA (Sigma, U.S.A.) during OGD.

Cell viability assay
Cell viability was assessed using the Cell Counting Kit-8 (CCK-8) assay. Cells were seeded in 96-well plates at a density of 5000 cells/well. At the designated time points, 10 µl of CCK-8 solution (Yeasen, China) was added to each well. The CCK-8 solution was mixed with the conditioned medium and incubated at 37 °C for approximately 2 h. Absorbance was measured at 450 nm using a multifunctional microplate reader (SpectraMax i3x, Japan).

Knockdown of USP14 gene in HT-22 cells
To knock down the expression of USP14 protein, a USP14 shRNA was developed to silence the USP14 gene. USP14 shRNA oligonucleotides with the LV2N (U6/Puro) vector were used to construct the Lenti-USP14 shRNA vectors. Lentiviruses (LentiUSP14 shRNA or Lenti-shRNA) (MOI = 10) were applied for transfecting HT-22 cells with 4 µg/ml polybrene for 24 h based on the manufacturer's directions (GenePharma, Shanghai, China). After 5 µg/ml puromycin selection, the HT-22 cells were harvested for Western blot to evaluate USP14 knockdown efficiency.

Apoptosis rate detection assay
The apoptosis rate was detected using Annexin V-APC/PI Apoptosis Kit (Multi Sciences Biotech, China). HT-22 cells were seeded in six-well plates at a density of 1×10^5 cells/well and cultured until reaching 90% confluence. After 6 h of OGD treatment, 5×10^4 cells were collected and resuspended in 300 µL of binding buffer. 5 µL of Annexin V-APC and 5 µL of PI staining solution were added, mixed well, and incubated for 5 minutes in the dark at room temperature. Samples were analyzed using a flow cytometer (BD Accuri™ C6 Plus, U.S.A.) within 1 h. Early apoptotic cells (Annexin V-APC-positive), late apoptotic cells (positive for both Annexin V-APC and PI), and necrotic cells (PI-positive) were sorted from the general cell population, and apoptosis rates were calculated from three replicate experiments.

Detection of mitochondrial membrane potential (ΔΨm)
Mitochondrial membrane potential was assessed using a JC-1 assay kit (MedChemExpress, USA) following the manufacturer's instructions. Briefly, cells were harvested using EDTA-free trypsin and transferred to centrifuge tubes. JC-1 working solution in culture medium was then added, and the cell suspension was incubated at 37 °C for 20 min, with gentle mixing every 5 min to ensure uniform staining. After incubation, cells were centrifuged at 400×g for 3 min at 4 °C, and the pellet was washed twice with PBS. The fluorescence signal was subsequently analyzed using flow cytometry (BD Accuri™ C6 Plus, USA).

Mitochondrial ROS detection
Mitochondrial reactive oxygen species (mtROS) were measured using the MitoSOX Red mitochondrial superoxide indicator (MedChemExpress, USA) in accordance with the manufacturer's protocol. The dye was diluted in serum-free medium to a final concentration of 2 µmol/L. Collected cells were resuspended in the working solution and incubated at 37 °C for 30 min, with gentle mixing every 10 min to ensure adequate staining. Following incubation, cells were centrifuged at 800 rpm for 3 min, washed twice with serum-free medium, and subsequently analyzed by flow cytometry (BD Accuri™ C6 Plus, USA).

Transmission electron microscopy
HT-22 cells were collected and fixed in 2% pre-cooled glutaraldehyde at 4 °C for 2 h. Following fixation, cells were stained with 2% uranyl acetate for another 2 h. Gradual dehydration was performed using a graded acetone series (50%, 70%, 90%, and 100%). The dehydrated samples were then embedded, sectioned into ultrathin slices, and examined by transmission electron microscopy (Hitachi HT7700, Japan).

Statistical analysis
All results are presented as means ± standard deviation (SD). Statistical analyses were conducted based on data obtained from at least three independent experiments, utilizing SPSS (version 25.0) and GraphPad Prism (version 10.0). Comparisons among multiple groups were performed using two-way ANOVA or one-way ANOVA, with subsequent Tukey's multiple comparison tests to identify significant differences. $p < 0.05$ was regarded as statistically significant.

Data availability
The datasets generated and/or analyzed during the current study are available from the corresponding author upon reasonable request.

Received: 14 September 2025; Accepted: 4 December 2025
Published online: 09 December 2025

References
1. Xu, S., Jia, J., Mao, R., Cao, X. & Xu, Y. Mitophagy in acute central nervous system injuries: regulatory mechanisms and therapeutic potentials. *Neural Regen Res.* **20**, 2437–2453 (2024).
2. Liu, S. et al. Disrupted autophagy after spinal cord injury is associated with ER stress and neuronal cell death. *Cell. Death Dis.* **6**, e1582–e1582 (2015).
3. Hu, X. et al. Spinal cord injury: molecular mechanisms and therapeutic interventions. *Signal. Transduct. Target. Ther.* **8**, 1–28 (2023).

4. Giacomello, M., Pyakurel, A., Glytsou, C. & Scorrano, L. The cell biology of mitochondrial membrane dynamics. *Nat. Rev. Mol. Cell. Biol.* **21**, 204–224 (2020).
5. Wedan, R. J., Longenecker, J. Z. & Nowinski, S. M. Mitochondrial fatty acid synthesis is an emergent central regulator of mammalian oxidative metabolism. *Cell. Metab.* **36**, 36–47 (2024).
6. Lamade, A. M. et al. Mitochondrial damage & lipid signaling in traumatic brain injury. *Exp. Neurol.* **329**, 113307 (2020).
7. Xu, B. et al. Exosomes derived from Schwann cells alleviate mitochondrial dysfunction and necroptosis after spinal cord injury via AMPK signaling pathway-mediated mitophagy. *Free Radic Biol. Med.* **208**, 319–333 (2023).
8. Jiang, D. et al. Zinc defends against parthanatos and promotes functional recovery after spinal cord injury through SIRT3-mediated anti-oxidative stress and mitophagy. *CNS Neurosci. Ther.* **29**, 2857–2872 (2023).
9. Wang, F., Ning, S., Yu, B. & Wang, Y. USP14: structure, function, and target Inhibition. *Front. Pharmacol.* **12**, 801328 (2022).
10. Xu, D. et al. USP14 regulates autophagy by suppressing K63 ubiquitination of Beclin 1. *Genes Dev.* **30**, 1718–1730 (2016).
11. Chakraborty, J. et al. USP14 Inhibition corrects an in vivo model of impaired mitophagy. *EMBO Mol. Med.* **10**, e9014 (2018).
12. Lee, B. H. et al. Enhancement of proteasome activity by a small-molecule inhibitor of USP14. *Nature* **467**, 179–184 (2010).
13. Wang, Z. et al. Inhibition of HSP90α protects cultured neurons from oxygen-glucose deprivation induced necroptosis by decreasing RIP3 expression. *J. Cell. Physiol.* **233**, 4864–4884 (2018).
14. Jiao, J., Wang, Y., Ren, P., Sun, S. & Wu, M. Necrosulfonamide ameliorates neurological impairment in spinal cord injury by improving antioxidative capacity. *Front. Pharmacol.* **10**, 1538 (2020).
15. Yang, J. et al. Mesoporous polydopamine delivering 8-gingerol for the target and synergistic treatment to the spinal cord injury. *J. Nanobiotechnol.* **21**, 192 (2023).
16. Zeng, L. et al. Melatonin attenuates ropivacaine-induced apoptosis by inhibiting excessive mitophagy through the parkin/PINK1 pathway in PC12 and HT22 cells. *Inflammation* **45**, 725–738 (2022).
17. Li, Q. et al. Rapamycin enhances mitophagy and attenuates apoptosis after spinal ischemia-reperfusion injury. *Front. Neurosci.* **12**, 865 (2018).
18. Wang, S. et al. A mitochondrion-targeting piezoelectric nanosystem for the treatment of erectile dysfunction via autophagy regulation. *Adv. Mater.* **37**, 2413287 (2024).
19. Bai, M. et al. Zinc ions regulate mitochondrial quality control in neurons under oxidative stress and reduce PANoptosis in spinal cord injury models via the Lgals3-bax pathway. *Free Radic Biol. Med.* **221**, 169–180 (2024).
20. Xue, J. L. et al. The multifaceted effects of mitochondria in kidney diseases. *Mitochondrion* **79**, 101957 (2024).
21. Yao, H. et al. Enhancing mitophagy by ligustilide through BNIP3-LC3 interaction attenuates oxidative stress-induced neuronal apoptosis in spinal cord injury. *Int. J. Biol. Sci.* **20**, 4382–4406 (2024).
22. Lin, J. et al. P2Y6R inhibition induces microglial M2 polarization by promoting PINK1/parkin-dependent mitophagy after spinal cord injury. *Mol. Neurobiol.* **62**, 7054–7074 (2024).
23. Kedra, J., Lin, S., Pacheco, A., Gallo, G. & Smith, G. M. Axotomy induces Drp1-dependent fragmentation of axonal mitochondria. *Front. Mol. Neurosci.* **14**, 668670 (2021).
24. Zhang, J. et al. Artesunate-induced mitophagy alters cellular redox status. *Redox Biol.* **19**, 263–273 (2018).
25. Gomes, L. C. & Scorrano, L. Mitochondrial morphology in mitophagy and macroautophagy. *Biochim. Biophys. Acta BBA - Mol. Cell. Res.* **1833**, 205–212 (2013).
26. Bo, Q. et al. 3-methyladenine alleviates experimental subretinal fibrosis by inhibiting macrophages and M2 polarization through the PI3K/akt pathway. *J. Ocul Pharmacol. Ther.* **36**, 618–628 (2020).
27. Ahuja, C. S. et al. Traumatic spinal cord injury. *Nat. Rev. Dis. Primer.* **3**, 1–21 (2017).
28. Alizadeh, A., Dyck, S. M. & Karimi-Abdolrezaee, S. Traumatic spinal cord injury: an overview of Pathophysiology, models and acute injury mechanisms. *Front. Neurol.* **10**, 282 (2019).
29. Lu, Y. et al. Global, regional, and National burden of spinal cord injury from 1990 to 2021 and projections for 2050: a systematic analysis for the global burden of disease 2021 study. *Ageing Res. Rev.* **103**, 102598 (2025).
30. Alcántar-Garibay, O. V., Incontri-Abraham, D. & Ibarra, A. Spinal cord injury-induced cognitive impairment: a narrative review. *Neural Regen Res.* **17**, 2649 (2022).
31. Pang, Q. M. et al. Multiple strategies enhance the efficacy of MSCs transplantation for spinal cord injury. *Biomed. Pharmacother.* **157**, 114011 (2023).
32. Wang, J. & Zhou, H. Mitochondrial quality control mechanisms as molecular targets in cardiac ischemia–reperfusion injury. *Acta Pharm. Sin B.* **10**, 1866–1879 (2020).
33. Yang, J. et al. Chemical Inhibition of mitochondrial fission via targeting the DRP1-receptor interaction. *Cell. Chem. Biol.* **30**, 278–294e11 (2023).
34. Liu, Z. et al. Advanced oxidation protein products induce microglia-mediated neuroinflammation via MAPKs-NF-κB signaling pathway and pyroptosis after secondary spinal cord injury. *J. Neuroinflammation.* **17**, 90 (2020).
35. He, Z. et al. Targeting mitochondrial oxidative stress: potential neuroprotective therapy for spinal cord injury. *J. Integr. Neurosci.* **22**, 153 (2023).
36. Chakrabarti, R. & Higgs, H. N. Revolutionary view of two ways to split a mitochondrion. *Nature* **593**, 346–347 (2021).
37. Slater, P. G., Domínguez-Romero, M. E., Villarreal, M., Eisner, V. & Larraín, J. Mitochondrial function in spinal cord injury and regeneration. *Cell. Mol. Life Sci.* **79**, 239 (2022).
38. Onishi, M., Yamano, K., Sato, M., Matsuda, N. & Okamoto, K. Molecular mechanisms and physiological functions of mitophagy. *EMBO J.* **40**, e104705 (2021).
39. Sprenger, H. G. & Langer, T. The good and the bad of mitochondrial breakups. *Trends Cell. Biol.* **29**, 888–900 (2019).
40. Lacombe, A. & Scorrano, L. The interplay between mitochondrial dynamics and autophagy: from a key homeostatic mechanism to a driver of pathology. *Semin Cell. Dev. Biol.* **161–162**, 1–19 (2024).
41. Tian, Z. et al. Self-healing COCu-tac hydrogel enhances iNSCs transplantation for spinal cord injury by promoting mitophagy via the FKBP52/AKT pathway. *Adv. Sci.* **12**, 2407757 (2024).
42. Mevissen, T. E. T. & Komander, D. Mechanisms of deubiquitinase specificity and regulation. *Annu. Rev. Biochem.* **86**, 159–192 (2017).
43. Clague, M. J., Urbé, S. & Komander, D. Breaking the chains: deubiquitylating enzyme specificity begets function. *Nat. Rev. Mol. Cell. Biol.* **20**, 338–352 (2019).
44. Tsefou, E. & Ketteler, R. Targeting deubiquitinating enzymes (DUBs) that regulate mitophagy via direct or indirect interaction with parkin. *Int. J. Mol. Sci.* **23**, 12105 (2022).
45. Liang, Y. et al. The role of ubiquitin–proteasome system and mitophagy in the pathogenesis of parkinson's disease. *NeuroMolecular Med.* **25**, 471–488 (2023).
46. Niu, K. et al. USP33 deubiquitinates PRKN/parkin and antagonizes its role in mitophagy. *Autophagy* **16**, 724–734 (2019).
47. Zhang, F. et al. Ruthenium red alleviates post-resuscitation myocardial dysfunction by upregulating mitophagy through Inhibition of USP33 in a cardiac arrest rat model. *Eur. J. Pharmacol.* **974**, 176633 (2024).
48. Fang, T. S. Z. et al. Knockout or Inhibition of USP30 protects dopaminergic neurons in a parkinson's disease mouse model. *Nat. Commun.* **14**, 7295 (2023).
49. Okarmus, J. et al. USP30 Inhibition induces mitophagy and reduces oxidative stress in parkin-deficient human neurons. *Cell. Death Dis.* **15**, 1–13 (2024).

50. Liu, Y. et al. Inhibition of USP30 promotes mitophagy by regulating ubiquitination of MFN2 by parkin to attenuate early brain injury after SAH. *Transl Stroke Res.* **16**, 448–466 (2023).
51. Greta, B. et al. USP14 Inhibition enhances parkin-independent mitophagy in iNeurons. *Pharmacol. Res.* **210**, 107484 (2024).
52. Lin, C., Li, L., Xu, Q., Xu, S. & Tang, C. Yap1-Usp14 axis inhibits neuronal mitophagy during neonatal hypoxia–ischemia encephalopathy by regulation of beclin-1 ubiquitination in mouse. *Mol. Neurobiol.* **60**, 4273–4287 (2023).
53. Xu, Y. H. & Guo, N. L. USP14 inhibitor IU1 prevents ventilator-induced lung injury in rats. *Cell. Mol. Biol.* **60**, 50–54 (2014).
54. Jia-Wei Min, L., Lü, J. L. & Freeling, D. S. Martin, & Hongmin Wang. USP14 inhibitor attenuates cerebral ischemia/reperfusion-induced neuronal injury in mice. *J. Neurochem*. **140**, 826–833 (2017).
55. Basso, D. M., Beattie, M. S. & Bresnahan, J. C. A sensitive and reliable locomotor rating scale for open field testing in rats. *J. Neurotrauma*. **12**, 1–21 (1995).
56. Basso, D. M., Beattie, M. S. & Bresnahan, J. C. Graded histological and locomotor outcomes after spinal cord contusion using the NYU weight-drop device versus transection. *Exp. Neurol.* **139**, 244–256 (1996).
57. Hemel, I. M. G. M., Engelen, B. P. H., Luber, N. & Gerards, M. A hitchhiker's guide to mitochondrial quantification. *Mitochondrion* **59**, 216–224 (2021).

Acknowledgements

We thank all the laboratory administrators in the Central Laboratory of Fujian Medical University Union Hospital for their kind guidance and help.

Author contributions

Conceptualization: D.W., D.C., H.C., Z.W., W.L.; Data Curation: D.W., D.C., H.C.; Formal Analysis: D.W., D.C., H.C.; Funding acquisition: Z.W., W.L.; Methodology: H.F., Z.Y., L.Z., T.S.; Project Administration: D.W., L.S., Z.W., W.L.; Visualization: D.W., D.C., H.C., R.W., Y.Z.; Writing – Original Draft: D.W., D.C., H.C.; Writing – Review & Editing: D.W., D.C., L.Z., Z.C., Z.W., W.L.

Funding

This study was supported by Joint Funds for the innovation of Science and Technology, Fujian province (Grant number: 2021Y9041), Fujian provincial health technology project (Grant number: 2023CXA013) and Fujian Natural Science Foundation (2023J01758).

Declarations

Competing interests

The authors declare no competing interests.

Ethics approval and consent to participate

All animal experimental procedures were approved by the Institutional Animal Care and Use Committee (IACUC) of Fujian Medical University with ethics approval number IACUC FJMU 2024 – 0137.

Additional information

Supplementary Information The online version contains supplementary material available at https://doi.org/10.1038/s41598-025-31745-0.

Correspondence and requests for materials should be addressed to Z.W. or W.L.